Supporting Information

Lai et al.

SI text

Experimental Results

Details of the mouse experiments of Fig. 3(a): Four to six week old immune competent Balb/c mice were injected subcutaneously in the mammary fat pad with 1×10^6 EMT6-HER2 murine mammary carcinoma cells. Mice were administered (1) vehicle, (2) BETi (PLX 51107) (20 mg/kg daily), via oral gavage, (3) anti-CTLA-4 antibody from Bio X Cell (clone 9H10) at 100 μg by twice weekly intraperitoneal injection or (4) the combination of BETi and anti-CTLA-4 antibody. Treatment started once tumor diameters reached 5 mm (approximately 7-10 days after tumor injection). Ten to eleven mice were included in each treatment group. Tumor volumes were measured three times weekly with digital calipers. Tumor volume was estimated by the following equation: Tumor volume $= 0.5 \times [(\text{larger diameter}) \times (\text{smaller diameter})^2]$. Values are the mean $\hat{A}\pm$ SE of tumor volumes at each time point.

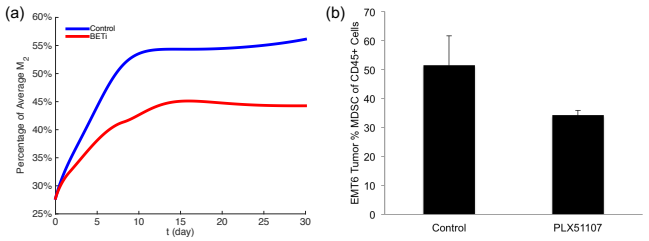

Fig. S1. Percentage of MDSC in CD45$^+$ Cells decreases under the treatment of BETi. (a) Numerical simulation results of BETi treatment with $\gamma_B = 1 \times 10^{-9}$ g/cm$^3 \cdot$ day. (b) EMT6 tumors were generated in Balb/c mice as described in Fig. S1A above and mice were treated with vehicle control or PLX 51107. Tumors were harvested at day 20, processed into single-cell suspensions and stained with Alexa 488 anti-GR-1 and APC anti-CD11b antibodies (BD Biosciences) to measure MDSC. Data were acquired using an LSRII flow cytometer and are expressed as percent of CD45$^+$ cells.

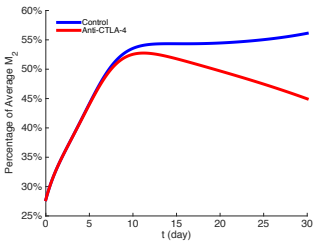

Fig. S2. Percentage of MDSC in CD45$^+$ Cells decreases under the treatment of anti-CTLA-4. Numerical simulation results of anti-CTLA-4 treatment with $\gamma_A = 0.9 \times 10^{-9}$ g/cm$^3 \cdot$ day.

Equation for DCs (D)

By necrotic cancer cells (N_C) we mean cancer cells undergoing the process of necrosis. Necrotic cancer cells release HMGB-1 (1). We model the dynamics of the necrotic cells (N_C) and HMGB-1 (H) by the following equations:

$$\frac{\partial N_C}{\partial t} + \underbrace{\nabla \cdot (\mathbf{u} N_C)}_{\text{velocity}} - \underbrace{\delta_{N_C} \nabla^2 N_C}_{\text{difusion}} = \underbrace{\lambda_{N_C C} C}_{\text{derived from life cancer cells}} - \underbrace{d_{N_C} N_C}_{\text{removal}},$$

$$\frac{\partial H}{\partial t} - \underbrace{\delta_H \nabla^2 H}_{\text{difusion}} = \underbrace{\lambda_{H N_C} N_C}_{\text{released from nerotic cancer cells}} - \underbrace{d_H H}_{\text{degradation}},$$

where $\lambda_{N_C C}$ is the rate at which cancer cells become necrotic and $\lambda_{H N_C}$ is the rate at which necrotic cells produce HMGB-1. We note that although molecules like HMGB-1, or other proteins, may be affected by the velocity $\mathbf{u}$, their diffusion coefficients are several order of magnitude larger than the diffusion coefficients of cells, hence their velocity term may be neglected. The degradation of HMGB-1 is fast ($\sim$0.01/day) (2), and we assume that the process of necrosis is also fast. We may then approximate the two dynamical equations by the steady state equations $\lambda_{N_C C} C - d_{N_C} N_C = 0$ and $\lambda_{H N_C} N_C - d_H H = 0$, so that H is proportional to C.

Dendritic cells are activated by HMGB-1 (3, 4). Hence, the activation rate of immature dendritic cells, with density D_0, is proportional to $D_0 \frac{H}{K_H + H}$, or to $D_0 \frac{C}{K_C + C}$, since H is proportional to C. Here, the Michaelis-Menten law is used to account for the limited rate of receptor recycling time which takes place in the process of DCs activation. Hence, the dynamics of DCs is given by

$$\frac{\partial D}{\partial t} + \underbrace{\nabla \cdot (\mathbf{u} D)}_{\text{velocity}} - \underbrace{\delta_D \nabla^2 D}_{\text{difusion}} = \underbrace{\lambda_{DC} D_0 \frac{C}{K_C + C}}_{\text{activation by HMGB-1}} - \underbrace{d_D D}_{\text{death}},$$

where δ_D is the diffusion coefficient and d_D is the death rate of DCs.

Equations for cytokines

Equation for IL-12 (I_{12}). The proinflammatory cytokine IL-12 is secreted by activated DCs (5, 6) and by M1 macrophages (7), so that

$$\frac{\partial I_{12}}{\partial t} - \delta_{I_{12}} \nabla^2 I_{12} = \underbrace{\lambda_{I_{12} D} D + \lambda_{I_{12} M_1} M_1}_{\text{production by DCs and M1}} - \underbrace{d_{I_{12}} I_{12}}_{\text{degradation}}. \quad [S1]$$

Equation for IL-2 (I_2). IL-2 is produced by activated CD4$^+$ T cells (T_1) (6). Hence,

$$\frac{\partial I_2}{\partial t} - \delta_{I_2} \nabla^2 I_2 = \underbrace{\lambda_{I_2 T_1} T_1}_{\text{production by } T_1} - \underbrace{d_{I_2} I_2}_{\text{degradation}}. \quad [S2]$$

Equation for TGF-β (T_β). TGF-β is produced by tumor cells (8), Tregs (9) and M2 macrophages (10–12):

$$\frac{\partial T_\beta}{\partial t} - \delta_{T_\beta} \nabla^2 T_\beta = \underbrace{\lambda_{T_\beta C} C + \lambda_{T_\beta T_r} T_r + \lambda_{T_\beta M_2} M_2}_{\text{production by cancer, Tregs and M2}} - \underbrace{d_{T_\beta} T_\beta}_{\text{degradation}}. \quad [S3]$$

Equation for IL-10 (I_{10}). IL-10 is produced by cancer cells and by M2 macrophages (8). Hence I_{10} satisfies the following equation:

$$\frac{\partial I_{10}}{\partial t} - \delta_{I_{10}}\nabla^2 I_{10} = \underbrace{\lambda_{I_{10}C}C + \lambda_{I_{10}M_2}M_2}_{\text{production by cancer and M2}} - \underbrace{d_{I_{10}}I_{10}}_{\text{degradation}}. \quad [S4]$$

Equation for TNF-α (T_α). TNF-α is produced by primarily M1 macrophages and BETi reduces the production of TNF-α by the macrophages (13). TNF-α is also produced by Th1 cells (14, 15). Hence

$$\frac{\partial T_\alpha}{\partial t} - \delta_{T_\alpha}\nabla^2 T_\alpha = \underbrace{\lambda_{T_\alpha M_1}M_1}_{\text{production by M1}} \cdot \underbrace{\frac{1}{1+B/K_{T_\alpha B}}}_{\text{inhibited by BETi}} + \underbrace{\lambda_{T_\alpha T_1}T_1}_{\text{production by Th1}} - \underbrace{d_{T_\alpha}T_\alpha}_{\text{degradation}}. \quad [S5]$$

Equation for NO (N). NO is produced by M2 macrophages (16, 17), so that

$$\frac{\partial N}{\partial t} - \delta_N\nabla^2 N = \underbrace{\lambda_{NM_2}M_2}_{\text{production by M2}} - \underbrace{d_N N}_{\text{degradation}}. \quad [S6]$$

Equation for oxygen (W). Oxygen is infused through blood (18, 19). We identify the blood concentration with the density of endothelial cells. Accordingly,

$$\frac{\partial W}{\partial t} - \delta_W\nabla^2 W = \underbrace{\lambda_{WE}E}_{\text{source from blood}} - \underbrace{d_W W}_{\text{consumed by cells}}, \quad [S7]$$

where $d_W W$ represents the take-up rate of oxygen by all the cells.

Equation for VEGF (G). VEGF is produced by cancer cells (18, 19) and M2 macrophages (7, 19). BETi treatment down-regulates the hypoxic transcriptome response of cancer cells including VEGF-A (20, 21). Hence the equation for G is given by

$$\frac{\partial G}{\partial t} - \delta_G\nabla^2 G = \lambda_{GC}C \underbrace{\frac{1}{1+B/K_{GB}}}_{\text{inhibited by BETi}} + \underbrace{\lambda_{GM_2}M_2}_{\text{production by M2}} - \underbrace{d_G G}_{\text{degradation}}. \quad [S8]$$

Equation for M-CSF (M_C). M-CSF is produced by cancer cells (22), so that

$$\frac{\partial M_C}{\partial t} - \delta_{M_C}\nabla^2 M_C = \underbrace{\lambda_{M_C C}C}_{\text{production by cancer}} - \underbrace{d_{M_C}M_C}_{\text{degradation}}. \quad [S9]$$

Equation for MCP-1 (M_P). MCP-1 is produced by cancer cells and by M2 macrophages under inducement by M-CSF (11, 22), so that

$$\frac{\partial M_P}{\partial t} - \delta_{M_P}\nabla^2 M_P = \underbrace{\lambda_{M_P C}C + \lambda_{M_P M_2}M_2\frac{M_C}{K_{M_C+M_C}}}_{\text{production by cancer and M2}} - \underbrace{d_{M_P}M_P}_{\text{degradation}}. \quad [S10]$$

Equation for CTLA-4 (P), B7 (L) and CTLA-4-B7 (Q).

CTLA-4 is a ligand expressed on $CD4^+$ T cells and $CD8^+$ T cells; its receptor B7 is on dendritic cells. The complex CTLA-4-B7 blocks the activity of T cells. We assume that the number of CTLA-4 per cell is the same for T_1 and T_8 cells. If we denote by ρ_P the ratio between the mass of one CTLA-4 protein to the mass of one T cell, then

$$P = \rho_P(T_1+T_8), \quad \rho_P = \text{constant},$$

we conclude that P satisfies the equation

$$\frac{\partial P}{\partial t} + \nabla\cdot(\mathbf{u}P) - \delta_T\nabla^2 P = \rho_P\left[\frac{\partial(T_1+T_8)}{\partial t} + \nabla\cdot(\mathbf{u}(T_1+T_8)) - \delta_T\nabla^2(T_1+T_8)\right],$$

or,

$$\begin{aligned}&\frac{\partial P}{\partial t} + \nabla\cdot(\mathbf{u}P) - \delta_T\nabla^2 P\\ =&\frac{P}{T_1+T_8}\left[\frac{(\lambda_{T_1I_{12}}T_{10}+\lambda_{T_8I_{12}}T_{80})I_{12}}{(K_{I_{12}}+I_{12})(1+I_{10}/K_{TI_{10}})(1+T_r/K_{TT_r})}\right.\\ &\left.+(\lambda_{T_1I_2}T_1+\lambda_{T_8I_2}T_8)\frac{I_2}{K_{I_2}+I_2}\right]\times\frac{1+\varepsilon_{TB}}{1+Q/K_{TQ}}\\ &-\rho_P(d_{T_1}T_1+d_{T_8}T_8),\end{aligned}$$

where Q is the density of the complex CTLA-4-B7, and $\rho_P = \frac{P}{T_1+T_8}$. When anti-CTLA-4 drug (A) is applied, CTLA-4 is depleted by A. Hence,

$$\begin{aligned}&\frac{\partial P}{\partial t} + \nabla\cdot(\mathbf{u}P) - \delta_T\nabla^2 P\\ =&\frac{P}{T_1+T_8}\left[\frac{(\lambda_{T_1I_{12}}T_{10}+\lambda_{T_8I_{12}}T_{80})I_{12}}{(K_{I_{12}}+I_{12})(1+I_{10}/K_{TI_{10}})(1+T_r/K_{TT_r})}\right.\\ &\left.+(\lambda_{T_1I_2}T_1+\lambda_{T_8I_2}T_8)\frac{I_2}{K_{I_2}+I_2}\right]\times\frac{1+\varepsilon_{TB}}{1+Q/K_{TQ}}\\ &-\frac{P}{T_1+T_8}(d_{T_1}T_1+d_{T_8}T_8) - \underbrace{\mu_{PA}P}_{\text{depletion by anti-CTLA-4}}.\end{aligned} \quad [S11]$$

The ligand B7 is expressed on dendritic cells, and we take

$$L = \rho_L D, \quad \rho_L = \text{constant}. \quad [S12]$$

CTLA-4 and B7 form the complex CTLA-4-B7 (Q) with association and disassociation rates α_{PL} and d_Q, respectively:

$$P + L \underset{d_Q}{\overset{\alpha_{PL}}{\rightleftharpoons}} Q. \quad [S13]$$

We assume that the half-life of Q is very short (23, 24), so that the dynamics in Eq. (S13) is in a quasi-steady state. Hence $\alpha_{PL}PL = d_Q Q$, or

$$Q = \sigma PL, \quad [S14]$$

where $\sigma = \alpha_{PL}/d_Q$.

Equation for cells velocity (u). We assume that the densities of cell in the growing tumor tend to steady state, and take the density of cancer cells in steady state to be [S16] g/cm^3. We also assume that most of the macrophages are "tumor associated macrophages" (TAM), which we identify as M2 macrophages. We accordingly take, in steady state, the density of M2 and M1 macrophages to be $M_2 = 3.2\times10^{-3}$ g/cm^3 and $M_1 = 10^{-4}$ g/cm^3.

We take the steady state density of endothelial cells to be $E = 2.5\times10^{-3}$ g/cm^3 (25), and as estimated in the parameter estimation section, the steady state densities of the immune cells D, T_1, T_8 and T_r to be (in unit of g/cm^3)

$$\begin{aligned}&D = 4\times10^{-4},\ T_1 = 2\times10^{-3},\ T_8 = 1\times10^{-3},\\ &T_r = 5\times10^{-4},\ M_1 = 1\times10^{-3},\ M_2 = 3.2\times10^{-3},\end{aligned} \quad [S15]$$

respectively. We assume that all cells have approximately the same volume and surface area, so that the diffusion coefficients

of all the cells are the same. Adding the equations of all the cells, we get

$$0.4097 \times \nabla \cdot \mathbf{u} = \sum_{j=2}^{9} [\text{right-hand side of Eq. j}], \qquad [S16]$$

where the constant 0.4097 follows from Eq. 1.

Boundary conditions We assume that the naive $CD4^+$ T cells and inactive $CD8^+$ T cells that migrated from the lymph nodes into the tumor microenvironment have constant densities $\hat{T}_1$ and $\hat{T}_8$ at the tumor boundary, and that T_1 and T_8 are activated by IL-12 upon entering the tumor. We then have the following flux conditions at the tumor boundary:

$$\frac{\partial T_1}{\partial r} + \sigma_T(I_{12})(T_1 - \hat{T}_1) = 0, \ \frac{\partial T_8}{\partial r} + \sigma_T(I_{12})(T_8 - \hat{T}_8) = 0,$$
$$\frac{\partial T_r}{\partial r} + \sigma_{T_r}(T_\beta)(T_r - \hat{T}_r) = 0, \quad \text{at } r = R(t), \qquad [S17]$$

where we take $\sigma_T(I_{12}) = \sigma_0 \frac{I_{12}}{I_{12}+K_{I_{12}}}$ and $\sigma_{T_r}(T_\beta) = \sigma_0 \frac{T_\beta}{T_\beta + K_{T_\beta}}$.

We impose a no-flux boundary condition for all the remaining variables:

$$\text{No-flux for } D, M_1, M_2, E, C, I_{12}, I_2, T_\beta, I_{10}, T_\alpha, N, W, G, M_C, M_P, L, A, \text{ and } B \text{ at } r = R(t). \qquad [S18]$$

It is tacitly assumed here that the receptors PD-1 and ligands PD-L1 become active only after the T cells are already inside the tumor.

Parameter estimation

Half-saturation. In an expression of the form $Y \frac{X}{K_X + X}$ where Y is activated by X, the half-saturation parameter K_X is taken to be the approximate steady state concentration of species X.

Diffusion coefficients. By (26), we have the following relation for estimating the diffusion coefficients of a protein p:

$$\delta_p = \frac{M_G^{1/3}}{M_p^{1/3}} \delta_G,$$

where M_G and δ_G are respectively the molecular weight and diffusion coefficient of VEGF, M_p is the molecular weight of p, and $M_G = 24$kDa (27) and $\delta_G = 8.64 \times 10^{-2}$ cm^2 day^{-1} (28). Since, $M_{I_2} = 17.6$kDa (29), $M_{I_{12}} = 70$kDa (30), $M_{T_\beta} = 25$kDa (31), $M_{I_{10}} = 20.5$kDa (32), $M_{T_\alpha} = 25.6$kDa (33), $M_{M_C} = 60.2$kDa (34), $M_{M_P} = 11$kDa (35), $M_A = 146.3$kDa (Durvalumab) (36) and $M_B = 457$Da (JQ1) (37), we get $\delta_{I_2} = 9.58 \times 10^{-2}$ cm^2 day^{-1}, $\delta_{I_{12}} = 6.05 \times 10^{-2}$ cm^2 day^{-1}, $\delta_{T_\beta} = 8.52 \times 10^{-2}$ cm^2 day^{-1}, $\delta_{I_{10}} = 9.11 \times 10^{-2}$ cm^2 day^{-1}, $\delta_{T_\alpha} = 8.46 \times 10^{-2}$ cm^2 day^{-1}, $\delta_{M_C} = 6.36 \times 10^{-2}$ cm^2 day^{-1}, $\delta_{M_P} = 1.12 \times 10^{-1}$ cm^2 day^{-1}, $\delta_A = 4.73 \times 10^{-2}$ cm^2 day^{-1} and $\delta_B = 3.24 \times 10^{-1}$ cm^2 day^{-1}.

Eq. 2. The number of DCs in various organs (heart, kidney, pancreas and liver) in mouse varies from 1.1×10^6 cells/cm^3 to 6.6×10^6 cells/cm^3 (38). In the dermal tissue, the number of DCs is larger (600-1500 cells/mm^2) (39, 40), but we do not specify where the melanoma cancer is located; it may be at its initial dermal tissue or in another organ where it metastasized. Mature DCs are approximately 10 to 15 μm in diameter (41). Accordingly, we estimate the steady state of DCs to be $K_D = 4 \times 10^{-4}$ g/cm^3. We assume that there are always immature dendritic cells, some coming from the blood as tumor infiltrating dendritic cells (TID) (5, 6, 42). We also assume that the density of immature DCs to be smaller than the density of active DCs, and take $D_0 = \frac{1}{20} K_D = 2 \times 10^{-5}$ g/cm^3.

If we use, as the steady state equation of Eq. 2, the relation $\lambda_{DC} D_0 \frac{C}{K_C + C} = d_D D$, where, $d_D = 0.1$/day (43), $C = K_C = 0.4$ g/cm^3, $D = K_D = 4 \times 10^{-4}$ g/cm^3, $D_0 = 2 \times 10^{-5}$ g/cm^3, we get $\lambda_{DC} = 2 d_D D / D_0 = 4$/day. We note however that in estimating λ_{DC}, we ignored the contribution of $\nabla \cdot (\mathbf{u} D)$, whose integral over the tumor $\{r < R(t)\}$ is $\int_{r=R(t)} \frac{dR(t)}{dt} \cdot D$, which is a positive quantity. Hence, $\frac{\partial D}{\partial t}$ is actually decreased when we equate to zero the right-hand side (RHS) of Eq. 2; we therefore need to increase λ_{DC}; we take $\lambda_{DC} = 10$/day.

Eqs. 3 and 4. The number of lymphocytes is approximately twice the number of DCs (38). T cells are approximately 5 to 10 μm in diameter. Assuming that the number of Th1 cells is 1/4 the number of lymphocytes, we estimate steady state density of Th1 cells to be $K_{T_1} = 2 \times 10^{-3}$ g/cm^3. We assume that the density of naive $CD4^+$ T cells to be less than the density of Th1, and take $T_{10} = \frac{1}{5} K_T = 4 \times 10^{-4}$ g/cm^3. We choose K_{TT_r} to be half of the half-saturation of T_r, that is, $K_{TT_r} = K_{T_r}/2 = 2.5 \times 10^{-4}$ g/cm^3, and $K_{TI_{10}}$ to be half of the half-saturation of I_{10}, namely, $K_{TI_{10}} = K_{I_{10}}/2 = 4.375 \times 10^{-11}$ g/cm^3. We assume that in steady state, $Q/K_{TQ} = 2$ (the value of K_{TQ} is derived in the estimates of Eqs. 20-22.

From the steady state of Eq. 2 (more precisely, by setting to zero the RHS of Eq. 2 without BETi, we get

$$\left(\lambda_{T_1 I_{12}} T_{10} \cdot \frac{1}{2} \cdot \frac{1}{3} \cdot \frac{1}{3} + \lambda_{T_1 I_2} T_1 \cdot \frac{1}{2}\right) \cdot \frac{1}{3} - d_{T_1} T_1 = 0,$$

where $\lambda_{T_1 I_2} = 0.25$/day (43), $d_{T_1} = 0.197$/day (43), $T_{10} = 4 \times 10^{-4}$ g/cm^3 and $T_1 = K_{T_1} = 2 \times 10^{-3}$ g/cm^3. Hence $\lambda_{T_1 I_{12}} = 27.96$/day.

The CD4/CD8 ratio in the blood is 2:1. We assume a similar ratio in tissue, and take $T_{80} = \frac{1}{2} T_{10} = 2 \times 10^{-4}$ g/cm^3. We also take steady state of T_8 to be the half of steady state of T_1, i.e., $K_{T_8} = \frac{1}{2} K_{T_1} = 1 \times 10^{-3}$ g/cm^3.

From the steady state of Eq. 4 (more precisely, by setting to zero the RHS of Eq. 4, we get

$$\left(\lambda_{T_8 I_{12}} T_{80} \cdot \frac{1}{2} \cdot \frac{1}{3} \cdot \frac{1}{3} + \lambda_{T_1 I_2} T_8 \cdot \frac{1}{2}\right) \cdot \frac{1}{3} - d_{T_8} T_8 = 0$$

where $\lambda_{T_8 I_2} = 0.25$/day (43), $d_{T_8} = 0.18$/day (43), $T_{80} = 2 \times 10^{-4}$ g/cm^3, $T_8 = K_{T_8} = 1 \times 10^{-3}$ g/cm^3. Hence $\lambda_{T_8 I_{12}} = 24.90$/day.

As in the case of Eq.2, we actually need to consider the contribution of $\nabla \cdot (\mathbf{u} T_1)$ to the steady state assumption, and also the contribution of the flux of T cells at the tumor boundary. Since the flux of T cells is positive on the boundary, we actually get two contributions from the left-hand side (LHS) of Eq. 28, a positive term from $\nabla \cdot (\mathbf{u} T_1)$ and a negative term from the flux of T_1. We assume they cancel each other, and retain the above value of $\lambda_{T_1 I_{12}}$. The same applies to the cases of T_8 .

Eq. 5. From the steady state of Eq. 5 without BETi, we get, $\lambda_{T_rT_\beta} \cdot \frac{1}{2}T_{10} - d_{T_r}T_r = 0$, where $T_{10} = 4 \times 10^{-4}$ g/cm^3, $T_r = K_{T_r} = 5 \times 10^{-4}$ g/cm^3 (43), and $d_{T_r} = 0.2$/day (43). Hence $\lambda_{T_rT_\beta} = 0.5$/day. As in the case of Eq. 2, we increase $\lambda_{T_rT_\beta}$ to $\lambda_{T_rT_\beta} = 1.5$/day.

Eqs. 6 and 7. In breast cancer, most of the macrophages are M2 macrophages (7, 44). Accordingly we take $K_{M_2} = 3.2 \times 10^{-3}$ g/cm^3 and $K_{M_1} = 10^{-4}$ g/cm^3 at half-saturation of M_2 and M_1, and $M_{20} = 1.2M_2 = 3.84 \times 10^{-3}$ g/cm^3 and $M_{10} = 1.2M_1 = 1.2 \times 10^{-4}$ g/cm^3. From steady state of Eqs. 6 and 7 (setting the right hands sides to zero), we get,

$$\frac{1}{2}\lambda_{M_1}(M_{10} - M_1) + \beta_{M_2}M_2 - \beta_{M_1}M_1 = d_{M_1}M_1,$$

and

$$\frac{1}{2}\lambda_{M_2}(M_{20} - M_2) + \beta_{M_1}M_1 - \beta_{M_2}M_2 = d_{M_2}M_2.$$

where $d_{M_1} = d_{M_2} = 0.015$/day (25, 45). We assume that more M1 macrophages convert to M2 macrophages, and that $\beta_{M_1}M_1 = 2\beta_{M_2}M_2$ and $\beta_{M_1M_1} = 10d_{M_1}M_1$ in steady state. Hence $\beta_{M_1} = 0.15$, $\beta_{M_2} = 2.34 \times 10^{-3}$, $\lambda_{M_1} = 2(d_{M_1}M_1 - \beta_{M_2}M_2 + \beta_{M_1}M_1)/(M_{10} - M_1) = 0.90$/day, and $\lambda_{M_2} = 2(d_{M_2}M_2 + \beta_{M_2}M_2 - \beta_{M_1}M_1)/(M_{20} - M_2) = 0.13$/day, in steady state. As in the case of Eq. 2, in the steady state we need to take into account the advection terms $\nabla \cdot (\mathbf{u}M_1)$ and $\nabla \cdot (\mathbf{u}M_2)$ and thus increase both λ_{M_1} and λ_{M_1}. Furthermore, since cancer cells are proliferating, the tumor associated macrophages will also increase, which means additional increase of λ_{M_2} and λ_{M_1}. We take $\lambda_{M_2} = 1.01$/day and $\lambda_{M_1} = 1.35$/day.

Eq. 8. Setting to zero the RHS of Eq.8 we get, $\lambda_E E(1 - E/E_M)(G - G_0) - d_E E = 0$, where $d_E = 0.69$/day $E_M = 5 \times 10^{-3}$ g/cm^3, $E = K_E = 2.5 \times 10^{-3}$ g/cm^3, $G = K_G = 7 \times 10^{-8}$ g/cm^3(see Eq. S8) and $G_0 = 3.65 \times 10^{-10}$ g/cm^3. Hence, $\lambda_E = 2d_E/(K_G - G_0) = 1.98 \times 10^7$ cm^3/g$\cdot$day. As in the case of Eq. 2, because of the positive contribution of the average of $\nabla \cdot (\mathbf{u}E)$ in the steady state, we need to increase λ_E, and we take $\lambda_E = 2.38 \times 10^7$/day.

Eq. 9. We take $d_C = 0.17$ day^{-1}, $C_M = 0.8$ g/cm^3 (43) and $\lambda_C = 1.6$/day (46). In the steady state of the control case (no anti-tumor drugs), We assume that C is approximately 0.4 g/cm^3, and $W = K_W = 4.65 \times 10^{-4}$ and $N = K_N = 2 \times 10^{-6}$ g/cm^3 (see the estimates of Eqs. S7 and S6) (ignoring the advection term). In the the control case, from the steady state of Eq. 9, we have

$$\lambda_C \cdot \frac{1}{2} \cdot \frac{1}{2} - (\eta_1 T_1 + \eta_8 T_8) \cdot \frac{1}{2} - d_C = 0.$$

Noting that T_8 cells kill cancer cells more effectively than T_1 cells, we take $\eta_8 = 5\eta_1$, so that (with $T_1 = K_{T_1} = 2 \times 10^{-3}$ g/cm^3 and $T_8 = K_{T_8} = 1 \times 10^{-3}$ g/cm^3), $\eta_1 = 2(\lambda_C/4 - d_C)/(T_1 + 5T_8) = 65.71$ cm^3/g$\cdot$day and $\eta_8 = 328.55$ cm^3/g$\cdot$day. In the control case, including the effect of the advection term and the fact that the tumor grows, we need to increase the growth rate of cancer cells; we take $\lambda_C = 1.92$/day. When BETi drug is applied, we take $K_{CB} = 10K_B = 8.02 \times 10^{-10}$ g/cm^3, by the estimation of K_B (in Eq. 11).

Eqs. S1. The serum level of IL-12 in melanoma patients varies from $7.5 \times 10^{-11} - 9.6 \times 10^{-11}$ g/cm^3 (47, 48). We assume that the IL-12 level in tissue is higher, and take $I_{12} = K_{I_{12}} = 8 \times 10^{-10}$ g/cm^3. We assume that the production rate of IL-12 is the same for DCs and M1 macrophages, so that $\lambda_{I_{12}D}D = \lambda_{I_{12}M_1}M_1$. From steady state of Eq. (S1), we get $\lambda_{I_{12}D}D + \lambda_{I_{12}M_1}M_1 - d_{I_{12}}I_{12} = 0$, where $d_{I_{12}} = 1.38$/day (43), $D = K_D = 4 \times 10^{-4}$ g/cm^3, $M_1 = K_{M_1} = 10^{-4}$ g/cm^3, and $I_{12} = K_{I_{12}} = 8 \times 10^{-10}$ g/cm^3. Hence, $\lambda_{I_{12}D} = d_{I_{12}}I_{12}/(2D) = 1.38 \times 10^{-6}$/day, $\lambda_{I_{12}M_1} = 5.52 \times 10^{-6}$/day.

Eq. S3. The half-life of TGF-β is about 2 min (49), that is, $t_{1/2} = 0.0014$ day, so that $d_{T_\beta} = \ln 2/t_{1/2} = 499.07$ day^{-1}. The concentration of serum TGF-β in melanoma is 2.68×10^{-14} g/cm^3 (50). We assume that the concentration of TGF-β in tissue is higher than in serum, and take $T_\beta = 2.68 \times 10^{-13}$ g/cm^3. From the steady state of Eq. S3 we have, $\lambda_{T_\beta C}C + \lambda_{T_\beta M_2}M_2 + \lambda_{T_\beta T_r}T_r = d_{T_\beta}T_\beta$, where $d_{T_\beta} = 499.07$ day^{-1}, $T_\beta = K_{T_\beta} = 2.68 \times 10^{-13}$ g/cm^3, $T_r = K_{T_r} = 5 \times 10^{-4}$ g/cm^3 by Eq. 1, $C = K_C = 0.4$ g/cm^3, $M_2 = 3.2 \times 10^{-3}$ g/cm^3 . According to (8, 12), tumor cells secrete more TGF-β than M2 macrophages, and we assume that $\lambda_{T_\beta C}C = 5\lambda_{T_\beta M_2}M_2$ and $\lambda_{T_\beta T_r}T_r = 5\lambda_{T_\beta C}C$. Thus $\lambda_{T_\beta C} = d_{T_\beta}T_\beta/(6.2C) = 5.39 \times 10^{-11}$ /day, $\lambda_{T_\beta M_2} = \lambda_{T_\beta C}C/(5M_2) = 1.35 \times 10^{-9}$/day, and $\lambda_{T_\beta T_r} = 5\lambda_{T_\beta C}C/T_r = 2.16 \times 10^{-7}$/day.

Eq. S4. The half-life of IL-10 ranges from 1.1 to 2.6 hours (51); we take it to be 2 hours, that is, $t_{1/2} = 0.08$ day, so that $d_{I_{10}} = 8.32$ day^{-1}. The concentration of serum IL-10 in tumor is 8.75×10^{-12} g/cm^3 (52). We assumed that the concentration of I_{10} in tissue is higher, and take $I_{12} = K_{I_{10}} = 8.75 \times 10^{-11}$ g/cm^3 . From the steady state of Eq. (S4) we have, $\lambda_{I_{10}C}C + \lambda_{I_{10}M_2}M_2 - d_{I_{10}}I_{10} = 0$, where $d_{I_{10}} = 8.32$ day^{-1}. Tumor cells secrete more I_{10} than macrophages (53); accordingly, we take $\lambda_{I_{10}C} = 10\lambda_{I_{10}M_2}$. Hence, in steady state, $\lambda_{I_{10}M_2} = d_{I_{10}}I_{10}/(11M_2) = 2.07 \times 10^{-8}$/day, $\lambda_{I_{10}C} = 10\lambda_{I_{10}M_2}M_2/C = 1.65 \times 10^{-9}$/day.

Eq. S5. The half-life of TNF-α is 18.2min (54), that is, $t_{1/2} = 0.0126$ day, so that $d_{T_\alpha} = \ln 2/t_{1/2} = 55.01$ day^{-1}. From steady state of Eq. S5, without BETi, we get $\lambda_{T_\alpha M_1}M_1 + \lambda_{T_\alpha T_1}T_1 - d_{T_\alpha}T_\alpha = 0$, where $M_1 = K_{M_1} = 10^{-4}$ g/cm^3, $T_1 = K_{T_1} = 2 \times 10^{-3}$ g/cm^3 and $T_\alpha = K_{T_\alpha} = 3 \times 10^{-11}$ g/cm^3 (55). TNF-α is produced primarily by macrophages (13, 15), and accordingly we assume that $\lambda_{T_\alpha M_1}M_1 = 5\lambda_{T_\alpha T_1}T_1$. Hence, $\lambda_{T_\alpha T_1} = d_{T_\alpha}T_\alpha/(6T_1) = 1.36 \times 10^{-7}$/day, and $\lambda_{T_\alpha M_1} = 5\lambda_{T_\alpha T_1}/M_1 = 1.36 \times 10^{-6}$/day. When BETi drug is applied, we take $K_{TaB} = 10K_B = 8.02 \times 10^{-10}$ g/cm^3.

Eq. S6. From steady state of Eq. S6, we get $\lambda_{NM_2}M_2 - d_N N = 0$, where $d_N = 198$/day (56), $N = K_N = 2 \times 10^{-6}$ g/cm^3 (56) and $M_2 = 3.2 \times 10^{-3}$ g/cm^3. Hence, $\lambda_{NM_2} = d_N N/M_2 = 0.12$/day.

Eq. S7. From steady state of Eq. S7, we get $\lambda_{WE}E - d_W W = 0$, where $\lambda_{WE} = 7 \times 10^{-2}$/day (25), $W = K_W = 4.65 \times 10^{-4}$ g/cm^3 (25), $E = K_E = 2.5 \times 10^{-3}$ g/cm^3 (57). Hence, $d_W = \lambda_{WE}E/W = 3.76 \times 10^{-1}$/day.

Eq. S8. From steady state of Eq. S8 without BETi, we get $(\lambda_{GC}C + \lambda_{GM_2}M_2) - d_G G = 0$, where $d_G = 12.6$/day (25), $G = K_G = 7 \times 10^{-8}$ g/cm^3 (25), $C = K_C = 0.4$ g/cm^3, $M_2 = K_{M_2} = 3.2 \times 10^{-3}$ g/cm^3. VEGF is mainly produced

by cancer cells, and we accordingly take $\lambda_{GC}C = 10\lambda_{GM_2}M_2$. Hence, $\lambda_{GM_2} = d_G G/(11M_2) = 2.5\times10^{-5}$/day and $\lambda_{GC} = 10\lambda_{GM_2}M_2/C = 2.0\times10^{-6}$/day. When BETi drug is applied, we take $K_{GB} = 10K_B = 8.02\times10^{-10}$ g/cm^3.

Eq. S9. From steady state of Eq.S9, we get $\lambda_{M_C C}C - d_{M_C}M_C = 0$, where $d_{M_C} = 4.8$/day (25), $M_C = K_{M_C} = 10^{-9}$ g/cm^3 (25) and $C = K_C = 0.4$ g/cm^3. Hence, $\lambda_{M_C C} = d_{M_C}M_C/C = 1.2\times10^{-8}$/day.

Eq. S10. From steady state of Eq. S10, we get $\lambda_{M_P M_2}M_2\cdot\frac{1}{2} + \lambda_{M_P C}C - d_{M_P}M_P = 0$, where $d_{M_P} = 1.73$/day (25), $M_P = K_{M_P} = 2\times10^{-7}$ g/cm^3 (25), $M_2 = K_{M_2} = 3.2\times10^{-3}$ g/cm^3 and $C = K_C = 0.4$ g/cm^3. MCP-1 is produced primarily by cancer cells and take $\lambda_{M_P C} = 10\lambda_{M_P M_2}$. Hence, $\lambda_{M_P M_2} = d_{M_P}M_P/(10.5M_2) = 1.2\times10^{-8}$/day, and $\lambda_{M_P C} = 10\lambda_{M_p M_2}/C = 8.24\times10^{-7}$/day.

Eqs. S11-S14. In order to estimate the parameters K_{TQ} (in Eq. 2), we need to determine the steady state concentrations of P and L in the control case (no drugs). To do that, we begin by estimating ρ_P and ρ_L.

By (58), the mass of one CTLA-4 is $m_{C_L} = 25$ kDa$=4.15\times10^{-20}$ g, and, by (59), the mass of one B7 is $m_B = 52.5$ kDa$=8.12\times10^{-20}$ g. We assume that the mass of one T cell (or dendritic cell) is $m_T = m_D = 10^{-9}$ g. There are 6000 CTLA-4 proteins on one T cell (T_1 or T_8) (60) and 4000 B7 proteins on one dendritic cell (24). Hence $\rho_P = 6000\times\frac{m_{C_L}}{m_T} = \frac{6000\times(4.15\times10^{-20})}{10^{-9}} = 2.49\times10^{-7}$, and $\rho_L = 4000\times\frac{m_B}{m_D} = \frac{4000\times(8.12\times10^{-20})}{10^{-9}} = 3.25\times10^{-7}$. Taking $T_1 = K_{T_1} = 2\times10^{-3}$ g/cm^3 and $T_8 = K_{T_8} = 1\times10^{-3}$ g/cm^3 (61), we get, in steady state of C_L,

$$\begin{aligned}K_P = P =&\rho_P(T_1+T_8)\\ =&(2.49\times10^{-7})\times[2\times10^{-3}+1\times10^{-3}]\\ =&7.47\times10^{-10}\text{g/cm}^3.\end{aligned}$$

We assume that in a steady state $D = 4\times10^{-4}$ g/cm^3 (61). From Eq. (S12) we then get, in steady state of B,

$$\begin{aligned}K_L = L =&\rho_L D = (3.25\times10^{-7})\times(4\times10^{-4})\\ =&1.3\times10^{-10}\text{g/cm}^3.\end{aligned}$$

In steady state with $P = K_P$, $L = K_L$ and $Q = K_Q$, we have, by Eq. (S14), $K_Q = \sigma K_P K_L$. We take $K_{TQ} = \frac{1}{2}K_Q = \frac{1}{2}\sigma K_P K_L$. Hence, $Q/K_{TQ} = PL/(\frac{1}{2}K_P K_L)$ with variables P and L, and

$$\frac{1}{1+Q/K_{TQ}} = \frac{1}{1+PL/(\frac{1}{2}K_P K_L)} = \frac{1}{1+PL/K'_{TQ}}$$

where $K'_{TQ} = \frac{1}{2}K_P K_L = \frac{1}{2}\times(7.47\times10^{-10})\times(1.3\times10^{-10}) = 4.86\times10^{-20}$ g^2/cm^6.

Eqs. 10-11. By (62), the half-life of anti-CTLA-4 (ipilimumab) is 14.7 days, so that $d_A = \frac{\ln 2}{14.7} = 0.047$ day^{-1}. We assume that 10% of A is used in blocking CTLA-4, while the remaining 90% degrades naturally. Hence, $\mu_{C_L A}C_L A/10\% = d_A A/90\%$, so that

$$\mu_{PA} = \frac{d_A}{9P} = \frac{0.047}{9\times(7.47\times10^{-10})} = 6.99\times10^6\ \text{cm}^3/\text{g}\cdot\text{day}.$$

The half-life of BET inhibitor (JQ1) is in the range of 0.1-1.4 hours (63, 64); we take it to be 1.2 hours, so that $d_B = \frac{\ln 2}{1.2/24} = 13.86$ day^{-1}. We assume that 10% of B is absorbed by cancer cells, while the remaining 90% degrades naturally, so that $(\mu_{BC}C+\mu_{BM_1}M_1)\frac{B}{K_B+B}/10\% = d_B B/90\%$, or $\mu_{BC}C + \mu_{BM_1}M_1 = 2d_B B/9$, where $C = K_C = 0.4$ g/cm^3, $M_1 = K_{M_1} = 10^{-4}$ g/cm^3. From Eq. 11, we get $B \geq \gamma_B/d_B$, and we assume that

$$B \sim \frac{10}{9}\cdot\frac{\gamma_B}{d_B},$$

where $d_B = 13.86$/day.

In mice experiment with BETi and PD-1, BETi was given daily and CTLA-4 inhibitor was given 3 times/week. For simplicity, we take $\hat{A}(t) = \gamma_A$ and $\hat{B}(t) = \gamma_B$ as constants. It is difficult to compare the amount of administering dose of BETi to the actual parameter γ_B which appears in Eq.11, because no information is available on the PK/PD of the drug. We arbitrarily take γ_B to be order of magnitude 10^{-9} g/cm$^3\cdot$day in the simulations. Hence, $B = K_B = 8.02\times10^{-11}$ g/cm^3 in steady state.

We assume that the absorption rates of BETi by cancer cells and M1 macrophages are the same, i.e., $\mu_{BC} = \mu_{BM_1}$, so that $\mu_{BC} = \mu_{BM_1} = \frac{2d_B B}{9(C+M_1)} = 6.17\times10^{-10}$/day.

By taking $\gamma_B = 0.15\times10^{-9}$ g/cm$^3\cdot$day and $\gamma_A = 1.5\times10^{-9}$ g/cm$^3\cdot$day, we find that the tumor volume growth agrees qualitatively with the our experimental results when we apply just one drug or a combination of drug. We shall accordingly take γ_B to vary in the range $0-0.32\times10^{-9}$ g/cm$^3\cdot$day and γ_A to vary in the range $0-1.5\times10^{-9}$ g/cm$^3\cdot$day. We choose $\varepsilon_B = 20/K_B = 2\times10^{10}$ cm^3/g in Eqs. 3 and 4.

Sensitivity analysis. We performed sensitivity analysis with respect to the tumor volume at day 30 for two sets of parameters. The first set consists of production parameters for cells, including λ_{DC}, $\lambda_{T_1 I_{12}}$, $\lambda_{T_8 I_{12}}$, $\lambda_{T_r T_\beta}$, λ_{M_1}, λ_{M_2}, λ_E, λ_{CW}, $\lambda_{T_\alpha M_1}$, $\lambda_{T_\alpha T_1}$. Following the method of (65), we performed Latin hypercube sampling and generated 5000 samples to calculate the partial rank correlation coefficients (PRCC) and the p-values with respect to the tumor volume at day 30. In sampling all the parameters, we took the range of each parameter from 1/2 to twice its value in Table S2. The results are shown in Fig. S3. Fig. S3 shows that if the production parameters of T_1, T_8 and (to lesser extend) M_1 and D increase then tumor volume will increase, whereas if the production parameters of Treg, endothelial cells and M_2 increase then the tumor volume will increase.

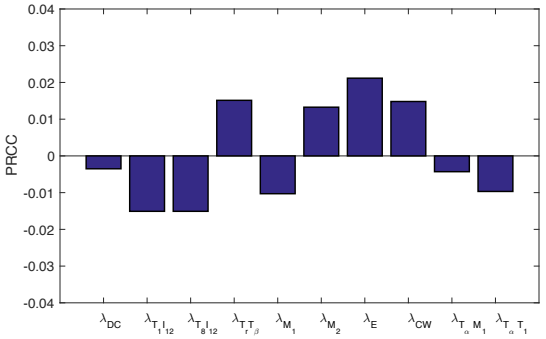

Fig. S3. Statistically significant PRCC values (p-value<0.01) for $R(t)$ at day 30.

The second set of parameters in the sensitivity analysis are β_{M_1}, β_{M_2}, η_8, η_1, K_{TQ}, ϵ_{TB}, K_{T_rB}, K_{CB}, $K_{T_\alpha B}$, K_{GB}, which play important roles in the dynamics of tumor cells. Here again we sampled all the parameters by taking the range of each parameter for 1/2 to twice its value in Tables S2 and S3. The results are shown in Fig. S4. Fig. S4 shows that the tumor volume decreases when the killing rates by T_1 and T_8 increase and when the inhibition of Q (represented by $1/K_{CB}$) decreases, whereas the tumor volume increases when inhibitions of T_r and C by BETi (represented by $1/K_{TQ}$) decrease.

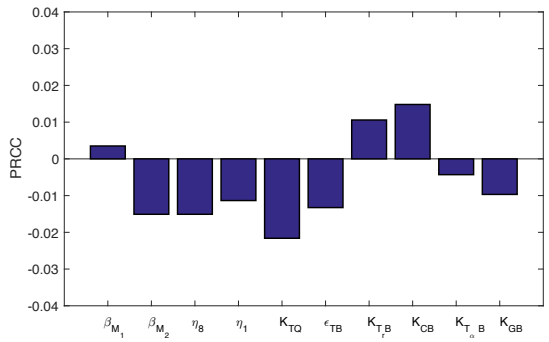

Fig. S4. Statistically significant PRCC values (p-value< 0.01) for $R(t)$ at day 30.

We also note that the switching parameters from β_{M_1} (from M_2 to M_1) and β_{M_2} (from M_1 to M_2) increase tumor volume as β_{M_1} increases and β_{M_2} decreases, but the effect of β_{M_2} is more significant.

Combination of BETi and anti-PD-L1

PD-1 is an immunoinhibitory receptor predominantly expressed on activated T cells (59, 66). Its ligand PD-L1 is upregulated on the same activated T cells, and is also expressed by myeloid-derived suppressor cells (MDSCs) (66–68) and in some human cancer cells (66, 67). Both PD-1 and PD-L1 are immune checkpoints: the complex PD-1-PD-L1 inhibits T cell function against cancer (59). It was recently shown that combining anti-PD-1 antibody with BETi (JQ1) is synergistic and leads to higher anti-tumor responses compared to each drug given alone (69). In the following we consider the combination of BETi (e.g. JQ1) and anti-PD-L1 (e.g. durvalumab). The model is similar to the model for combination of BETi and anti-CTLA-4, with some changes given below.

Equation for activated Tregs (T_r). The complex PD-1-PD-L1 enhances the expression of PTEN, which results in upregulation of Fox3+ in naive T cells, inducing them to differentiate into Tregs (T_r) (70). The production of T_r is also enhanced by TGF-β (T_β) (9, 11). Hence,

$$\frac{\partial T_r}{\partial t} + \nabla\cdot(\mathbf{u}T_r) - \delta_T\nabla^2 T_r = T_{10}\underbrace{\left(\lambda_{T_rT_\beta}\frac{T_\beta}{K_{T_\beta}+T_\beta}\right)}_{\text{TGF-}\beta\text{ induced proliferation}} + \underbrace{\lambda_{T_r\tilde{Q}}\frac{\tilde{Q}}{K_{\tilde{Q}}+\tilde{Q}}}_{\text{promotion by PD-1-PD-L1}} - \underbrace{d_{T_r}T_r}_{\text{death}}. \quad [S19]$$

Equation for PD-1 ($\tilde{P}$), PD-L1 ($\tilde{L}$) and PD-1-PD-L1 ($\tilde{Q}$). PD-1 is expressed on the surface of activated CD4$^+$ T cells, activated CD8$^+$ T cells and Tregs (59, 66). We assume that the number of PD-1 per cell is the same for T_1 and T_8 cells, but is smaller, by a factor ε_T, for T_r cells. If we denote by $\rho_{\tilde{P}}$ the ratio between the mass of one PD-1 protein to the mass of one T cell, then

$$\tilde{P} = \rho_{\tilde{P}}(T_1 + T_8 + \varepsilon_T T_r). \quad [S20]$$

PD-L1 is expressed on the surface of activated CD4$^+$ T cells, activated CD8$^+$ T cells (66), Tregs (71), M2 macrophages (66, 67) , and cancer cells (66, 67). We assume that the number of PD-L1 per cell is the same for T_1 and T_8 cells, and denote the ratio between the mass of one PD-L1 protein to the mass of one cell by $\rho_{\tilde{L}}$. Then

$$\tilde{L} = \rho_{\tilde{L}}(T_1 + T_8 + \varepsilon_T T_r + \varepsilon_M M_2 + \varepsilon_C C),$$

where ε_C and ε_M depend on the specific type of tumor.

The coefficient $\rho_{\tilde{L}}$ is constant when no anti-PD-L1 drug is administered. And in this case, $\tilde{L}$ satisfies the equation

$$\frac{\partial \tilde{L}}{\partial t} + \nabla\cdot(\mathbf{u}\tilde{L}) - \delta_T\nabla^2\tilde{L} = \rho_{\tilde{L}}\Big[\frac{\partial(T_1+T_8+\varepsilon_T T_r+\varepsilon_M M_2+\varepsilon_C C)}{\partial t} + \nabla\cdot(\mathbf{u}(T_1+T_8+\varepsilon_T T_r+\varepsilon_M M_2+\varepsilon_C C)) - \delta_T\nabla^2(T_1+T_8+\varepsilon_T T_r+\varepsilon_M M_2+\varepsilon_C C)\Big].$$

Recalling the equations of cells, we get

$$\frac{\partial \tilde{L}}{\partial t} + \nabla\cdot(\mathbf{u}\tilde{L}) - \delta_T\nabla^2\tilde{L} = \rho_{\tilde{L}}\,[\text{RHS of Eq. 3} + \text{RHS of Eq. 4} + \varepsilon_T \times \text{RHS of Eq. S19} + \varepsilon_M \times \text{RHS of Eq. 7} + \varepsilon_C \times \text{RHS of Eq. 9}]$$

with Q replaced by $\tilde{Q}$ in Eqs. 3 and 4.

When anti-PD-L1 drug ($\tilde{A}$) is applied, PD-L1 is depleted (or blocked) by $\tilde{A}$. In this case, the ratio $\frac{\tilde{L}}{T_1+T_8+\varepsilon_T T_r+\varepsilon_M M_2+\varepsilon_C C}$ may change. In order to include in the model both cases of with and without anti-PD-L1, we replace $\rho_{\tilde{L}}$ in the previous equation by $\frac{\tilde{L}}{T_1+T_8+\varepsilon_T T_r+\varepsilon_M M_2+\varepsilon_C C}$. Hence,

$$\frac{\partial \tilde{L}}{\partial t} + \nabla\cdot(\mathbf{u}\tilde{L}) - \delta_T\nabla^2\tilde{L} = \frac{\tilde{L}}{T_1+T_8+\varepsilon_T T_r+\varepsilon_M M_2+\varepsilon_C C} \times [\text{RHS of Eq. 3} + \text{RHS of Eq. 4} + \varepsilon_T \times \text{RHS of Eq. S19} + \varepsilon_M \times \text{RHS of Eq. 7} + \varepsilon_C \times \text{RHS of Eq. 9}] - \underbrace{\mu_{\tilde{L}\tilde{A}}\tilde{L}\tilde{A}}_{\text{depletion by anti-PD-L1}},$$

where $\mu_{\tilde{L}\tilde{A}}$ is the depletion rate of PD-L1 by anti-PD-L1.

When BETi is applied, the expression of PD-L1 by cancer cells is suppressed (69, 72), so that

$$\tilde{L} = \rho_{\tilde{L}}\left(T_1 + T_8 + \varepsilon_T T_r + \varepsilon_M M_2 + \varepsilon_C C\frac{1}{1+B/K_{\tilde{L}B}}\right).$$

When the two drugs are combined, the equation for L takes the form

$$\begin{aligned}\frac{\partial \tilde{L}}{\partial t} &+ \nabla\cdot(\mathbf{u}\tilde{L}) - \delta_T\nabla^2\tilde{L} \\ &= \frac{\tilde{L}}{T_1+T_8+\varepsilon_T T_r+\varepsilon_M M_2+\varepsilon_C C/(1+B/K_{\tilde{L}B})} \\ &\times [\text{RHS of Eq. 3} + \text{RHS of Eq. 4} \\ &+ \varepsilon_T \times \text{RHS of Eq. S19} + \varepsilon_M \times \text{RHS of Eq. 7} \\ &+ \varepsilon_C\frac{1}{1+B/K_{LB}} \times \text{RHS of Eq. 9}] \\ &- \underbrace{\mu_{\tilde{L}\tilde{A}}\tilde{L}\tilde{A}}_{\text{depletion by anti-PD-L1}}.\end{aligned} \quad [S21]$$

Note that in this equation we did not include the derivative of $\frac{1}{1+B/K_B}$ since, in equation of B (Eq. 11), d_B is large (see the estimates of Eq. 11) and hence $\frac{dB}{dt}$ is very small.

PD-L1 from T cells, M2 macrophages or cancer cells combines with PD-1 on the plasma membrane of T cells, to form a complex PD-1-PD-L1 ($\tilde{Q}$) on the T cells (66, 67). Denoting the association and disassociation rates of Q by $\alpha_{\tilde{P}\tilde{L}}$ and $d_{\tilde{Q}}$, respectively, we can write

$$\tilde{P} + \tilde{L} \underset{d_{\tilde{Q}}}{\overset{\alpha_{\tilde{P}\tilde{L}}}{\rightleftharpoons}} \tilde{Q}.$$

The half-life of $\tilde{Q}$ is less then 1 second (i.e. 1.16×10^{-5} day) (23), so that $d_{\tilde{Q}}$ is very large. Hence we may approximate the dynamical equation for $\tilde{Q}$ by the steady state equation, $\alpha_{\tilde{P}\tilde{L}}\tilde{P}\tilde{L} = d_{\tilde{Q}}\tilde{Q}$, or

$$\tilde{Q} = \tilde{\sigma}\tilde{P}\tilde{L}, \qquad [S22]$$

where $\tilde{\sigma} = \alpha_{\tilde{P}\tilde{L}}/d_{\tilde{Q}}$.

Parameter estimation for the anti-PD-L1 model.

Diffusion coefficients. $M_{\tilde{A}}$ = 146.3kDa (Durvalumab) (36) , hence $\delta_{\tilde{A}} = 4.73 \times 10^{-2}$ cm^2 day^{-1}.

Eq. S19. We assume that TGF-β activates Tregs more than PD-1-PD-L1 does, and take $\lambda_{T_rT_\beta} = 5\lambda_{T_r\tilde{Q}}$. From the steady state of Eq. 5, we get, $(\lambda_{T_rT_\beta} \cdot \frac{1}{2} + \lambda_{T_r\tilde{Q}} \cdot \frac{1}{2})T_{10} - d_{T_r}T_r = 0$, where $T_{10} = 1 \times 10^{-3}$ g/cm^3, $T_r = K_{T_r} = 5 \times 10^{-4}$ g/cm^3 (43), and $d_{T_r} = 0.2$/day (43). Hence $\lambda_{T_r\tilde{Q}} = 0.083$/day and $\lambda_{T_rT_\beta} = 0.415$/day.

Eqs. S20-S22. In order to estimate the parameters $K_{T\tilde{Q}}$ (in Eqs. 3 and 4 and $K_{\tilde{Q}}$ (in Eq. 5 with Q replaced by $\tilde{Q}$), we need to determine the steady state concentrations of $\tilde{P}$ and $\tilde{L}$ in the control case (no drugs). To do that, we begin by estimating $\rho_{\tilde{P}}$ and $\rho_{\tilde{L}}$.

By (58), the mass of one PD-1 is $m_{\tilde{P}} = 8.3\times10^{-8}$ pg=8.3×10^{-20} g, and by (59) the mass of one PD-L1 is $m_{\tilde{L}} = 5.8\times10^{-8}$ pg=5.8×10^{-20} g. We assume that the mass of one T cell is $m_T = 10^{-9}$ g. By (24), there are 3000 PD-1 proteins and 9000 PD-L1 proteins on one T cell (T_1 or T_8). Since $\rho_{\tilde{P}}T$ is the density of PD-1 (without anti-PD-1 drug), we get $\rho_{\tilde{P}} = 3000 \times \frac{m_{\tilde{P}}}{m_T} = \frac{3000\times(8.3\times10^{-20})}{10^{-9}} = 2.49 \times 10^{-7}$, and $\rho_L = 9000 \times \frac{m_{\tilde{L}}}{m_T} = \frac{9000\times(5.8\times10^{-20})}{10^{-9}} = 5.22 \times 10^{-7}$. PD-1 is expressed by Tregs at higher or lower level than in T_1 and T_8 cells depending on the type of the cancer (73); we assume that $\varepsilon_T = 0.8$. Hence, in steady state,

$$\begin{aligned}\tilde{P} &= \rho_{\tilde{P}}(T_1 + T_8 + \varepsilon_T T_r)\\ &= (2.49 \times 10^{-7}) \times [2 \times 10^{-3} + 1 \times 10^{-3} + 0.8 \times (5 \times 10^{-4})]\\ &= 8.46 \times 10^{-10}\text{g/cm}^3.\end{aligned}$$

The parameter ε_C in Eq. S21 depends on the type of cancer. We take $\varepsilon_C = 0.01$ (74), and $\varepsilon_M = 0.005$. Then, by Eq. S21, we get

$$\begin{aligned}K_{\tilde{L}} = \tilde{L} &= \rho_{\tilde{L}}(T_1 + T_8 + \varepsilon_M M + \varepsilon_C C)\\ &= (5.22 \times 10^{-7}) \times [3 \times 10^{-3} + 0.005 \times 0.4 + 0.01 \times 0.4]\\ &= 4.7 \times 10^{-9}\text{g/cm}^3.\end{aligned}$$

In steady state with $\tilde{P} = K_{\tilde{P}}$, $\tilde{L} = K_{\tilde{L}}$ and $\tilde{Q} = K_{\tilde{Q}}$, we have, by Eq. S22, $K_{\tilde{Q}} = \sigma K_{\tilde{P}}K_{\tilde{L}}$. We take $K_{T\tilde{Q}} = \frac{1}{2}K_{\tilde{Q}} = \frac{1}{2}\sigma K_{\tilde{P}}K_{\tilde{L}}$. Hence, $\tilde{Q}/K_{T\tilde{Q}} = \tilde{P}\tilde{L}/(\frac{1}{2}K_{\tilde{P}}K_{\tilde{L}})$ and we then have in Eqs. 3 and 4,

$$\frac{1}{1+\tilde{Q}/K_{T\tilde{Q}}} = \frac{1}{1+\tilde{P}\tilde{L}/(\frac{1}{2}K_{\tilde{P}}K_{\tilde{L}})} = \frac{1}{1+\tilde{P}\tilde{L}/K'_{T\tilde{Q}}},$$

where $K'_{T\tilde{Q}} = \frac{1}{2}K_{\tilde{P}}K_{\tilde{L}} = \frac{1}{2} \times (8.46 \times 10^{-10}) \times (4.7 \times 10^{-9}) = 1.99 \times 10^{-18}$ g^2/cm^6. Similarly, we have in Eq. S19,

$$\frac{\tilde{Q}}{K_{\tilde{Q}}+\tilde{Q}} = \frac{1}{1+K_{\tilde{Q}}/\tilde{Q}} = \frac{1}{1+K_{\tilde{P}}K_{\tilde{L}}/\tilde{P}\tilde{L}} = \frac{1}{1+K'_{\tilde{Q}}/\tilde{P}\tilde{L}}.$$

where $K'_{\tilde{Q}} = K_{\tilde{P}}K_{\tilde{L}} = 3.98 \times 10^{-18}$ g^2/cm^6. Similarly, when BETi drug is applied, it reduces the expression of PD-L1 on cancer cells by a factor $1/(1 + B/K_{\tilde{L}B})$ where we take $K_{\tilde{L}B} = 2K_B = 1.64 \times 10^{-10}$ g/cm^3.

Eqs. 10-11. By (75), the half-life of anti-PD-L1 is 15 days, so that $d_A = \frac{\ln 2}{15} = 0.046$ day^{-1}. We assume that 10% of A is used in blocking PD-L1, while the remaining 90% degrades naturally. Hence, $\mu_{LA}LA/10\% = d_AA/90\%$, so that

$$\mu_{LA} = \frac{d_A}{9L} = \frac{0.046}{9 \times (4.7 \times 10^{-9})} = 1.09 \times 10^6\ \text{cm}^3/\text{g} \cdot \text{day}.$$

By taking $\gamma_A = 5 \times 10^{-9}$ g/cm^3 $\cdot$ day and $\gamma_B = 0.2 \times 10^{-9}$ g/cm^3 $\cdot$ day, we find that the tumor volume growth agrees qualitatively with the experimental results in (76, 77) when we apply just one drug or a combination of drug. We shall accordingly take γ_B to vary in the range $0-5\times10^{-9}$ g/cm$^3\cdot$day and γ_A to vary in the range $0 - 8 \times 10^{-9}$ g/cm^3 $\cdot$ day.

Results. Figure S5-(A) shows that BETi, and anti-PD-L1 as single agents reduce tumor volume, and in combination the reduction by more than 75% at day 30.

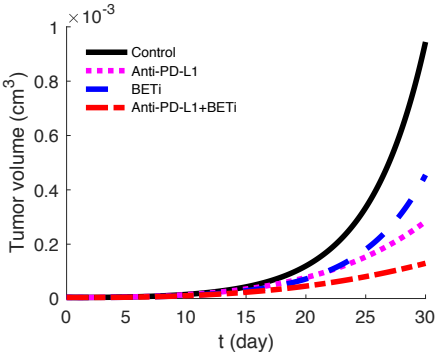

Fig. S5. The growth of tumor volume during the administration of anti-PD-L1 drug and BETi. Numerical simulation result with anti-PD-L1 is administered at rate $\gamma_{\tilde{A}} = 5 \times 10^{-9}$ g/cm^3 $\cdot$ day and BETi is administered at rate $\gamma_B = 0.6 \times 10^{-9}$ g/cm^3 $\cdot$ day. All other parameter values are the same as in Tables S2, S3 and S4.

Fig. S6 is the efficacy map of the combined therapy, with γ_B in the range of $0 - 0.2 \times 10^{-9}$ g/cm^3 $\cdot$ day and $\gamma_{\tilde{A}}$ in the range of $0-1.8\times10^{-9}$ g/cm$^3\cdot$day. The color column shows the efficacy for any pair of (γ_B, γ_A); the maximum efficacy is 0.98 (98%). We see that the two drugs are positively correlated in the sense that tumor volume decreases as each of the drugs is increased. Fig. S7 shows the average concentration of TNF-α, $T\alpha_{30}(\gamma_B, \gamma_{\tilde{A}})$, at day 30 under combined therapy with anti-PD-L1 (γ_A) and BETi (γ_B). We conclue, as in the case of anti-CTLA-4, that in order to achieve a largest tumor volume reduction with minimum TNF-α we should take a pair (γ_B, γ_A) with the smallest γ_B.

Since BETi suppresses PD-L1 expression by tumor cells (72), but may not suppress CTLA-4 expression, we carried

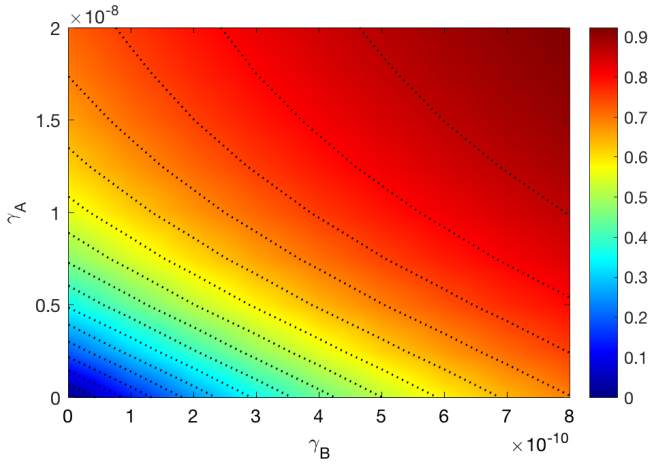

Fig. S6. Drug efficacy map. The color column shows the efficacy $E(\gamma_B, \gamma_A)$ when γ_B varies between $0 - 0.2 \times 10^{-9}$ g/cm$^3 \cdot$ day and γ_A varies between $0 - 1.8 \times 10^{-9}$ g/cm$^3 \cdot$ day. All other parameter values are the same as in Tables S2, S3 and S4.

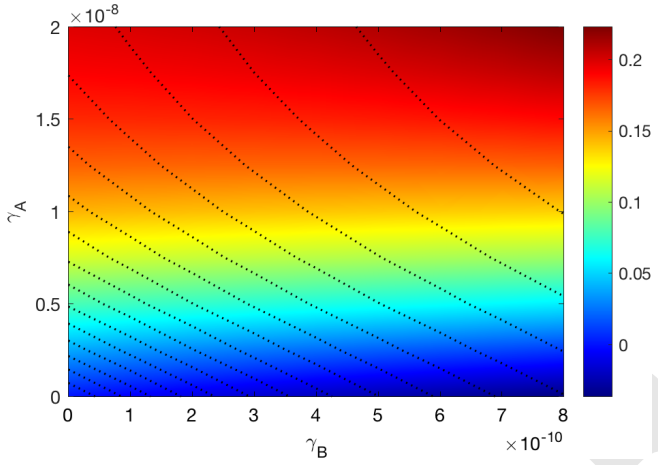

Fig. S7. Average density of TNF-α. The color column shows the 'adverse effect' function $AE(\gamma_B, \gamma_A)$ when γ_B varies between $0 - 0.2 \times 10^{-9}$ g/cm$^3 \cdot$ day and γ_A varies between $0 - 1.8 \times 10^{-9}$ g/cm$^3 \cdot$ day. All other parameter values are the same as in Tables S2, S3 and S4.

out murine study with combination of BETi and anti-CTLA-4 only.

The above model with small modifications applies extends to combination therapy with BETi and anti-PD-1.

Computational method

We employ moving mesh method (78) to numerically solve the free boundary problem for the tumor proliferation model. To illustrate this method, we take Eq. 2 as example and rewrite it as the following form:

$$\frac{\partial D(r,t)}{\partial t} = \delta_D \Delta D(r,t) - div(\mathbf{u}D) + F, \qquad [S23]$$

where F represents the term in the right hand side of Eq. 2. Let r_i^k and D_i^k denote numerical approximations of i-th grid point and $D(r_i^k, n\tau)$, respectively, where τ is the size of time-step. The discretization of Eq. S23 is derived by the fully implicit finite difference scheme:

$$\frac{D_i^{k+1} - D_i^k}{\tau} = \delta_D \left(D_{rr} + \frac{2}{r_i^k} D_r \right) - \left(\frac{2}{r_i^{k+1}} u_i^{k+1} + u_r \right) D_i^{k+1} - u_i^{k+1} D_r + F_i^{k+1}, \qquad [S24]$$

where $D_r = \frac{h_{-1}^2 D_{i+1}^{k+1} - h_1^2 D_{i-1}^{k+1} - (h_1^2 - h_{-1}^2) D_i^{k+1}}{h_1 (h_{-1}^2 - h_1 h_{-1})}$, $D_{rr} = 2 \frac{h_{-1} D_{i+1}^{k+1} - h_1 D_{i-1}^{k+1} + (h_1 - h_{-1}) D_i^{k+1}}{h_1 (h_1 h_{-1} - h_{-1}^2)}$, $u_r = \frac{h_{-1}^2 u_{i+1}^{k+1} - h_1^2 u_{i-1}^{k+1} - (h_1^2 - h_{-1}^2) u_i^{k+1}}{h_1 (h_{-1}^2 - h_1 h_{-1})}$, $h_{-1} = r_{i-1}^{k+1} - r_i^{k+1}$ and $h_1 = r_{i+1}^{k+1} - r_i^{k+1}$. The mesh moves by $r_i^{k+1} = r_i^k + u_i^{k+1}\tau$, where u_i^{k+1} is solved by the velocity equation.

1. Sims GP, Rowe DC, Rietdijk ST, Herbst R, Coyle AJ (2010) Hmgb1 and rage in inflammation and cancer. *Annu Rev Immunol* 28:367–388.
2. Zandarashvili L, et al. (April 2013) Real-time kinetics of high-mobility group box 1 (hmgb1) oxidation in extracellular fluids studied by in situ protein nmr spectroscopy. *J Biol Chem* 288(17):11621–11627.
3. Palucka J, Banchereau J (Mar 2012) Cancer immunotherapy via dendritic cells. *Nat Rev Cancer* 12(4):265–277.
4. Saenz R, et al. (Aug 2014) Tlr4-dependent activation of dendritic cells by an hmgb1-derived peptide adjuvant. *J Transl Med* 12(211):1–11.
5. Janco JMT, Lamichhane P, Karyampudi L, Knutson KL (Apr 2015) Tumor-infiltrating dendritic cells in cancer pathogenesis. *J Immunol* 194(7):2985–2991.
6. Ma Y, Shurin1 GV, Peiyuan Z, Shurin MR (2013) Dendritic cells in the cancer microenvironment. *J Cancer* 4(1):36–44.
7. Obeid E, Nanda R, Fu YX, Olopade OI (Jul 2013) The role of tumor-associated macrophages in breast cancer progression (review). *Int J Oncol* 43(1):5–12.
8. Perrot CY, Javelaud D, Mauviel A (May 2013) Insights into the transforming growth factor-beta signaling pathway in cutaneous melanoma. *Ann Dermatol* 25(2):135–144.
9. Whiteside TL (Augest 2015) The role of regulatory t cells in cancer immunology. *Immunotargets Ther* 4:159–171.
10. Condamine T, Gabrilovich DI (January 2011) Molecular mechanisms regulating myeloid-derived suppressor cell differentiation and function. *Trends Immunol* 32(1):19–25.
11. Umansky V, Blattner C, Gebhardt C, , Utikal J (November 2016) The role of myeloid-derived suppressor cells (mdsc) in cancer progression. *Vaccines* 4(36):1–16.
12. Cantelli G, Crosas-Molist1 E, Georgouli M, Sanz-Moreno V (Augest 2016) Tgfb-induced transcription in cancer. *Seminars in Cancer Biology* p. http://dx.doi.org/10.1016/j.semcancer.2016.08.009.
13. Belkina AC, Nikolajczyk BS, , Denis GV (Apr 2013) Bet protein function is required for inflammation: Brd2 genetic disruption and bet inhibitor jq1 impair mouse macrophage inflammatory responses. *J Immunol* 190(7):3670–3678.
14. Jiandong Zhang, Mehul B. Patel RGAMYsSNSK, , et al. (Dec 2014) Tumor necrosis factor-alpha produced in the kidney contributes to angiotensin ii-dependent hypertension. *Hypertension* 64(6):1275–1281.
15. Chen X, Oppenheim JJ (Dec 2011) Contrasting effects of tnf and anti-tnf on the activation of effector t cells and regulatory t cells in autoimmunity. *FEBS Lett* 585(23):3611–3618.
16. Gabrilovich DI, Nagaraj S (Mar 2009) Myeloid-derived suppressor cells as regulators of the immune system. *Nat Rev Immunol* 9(3):162–74.
17. Gabrilovich DI, Ostrand-Rosenberg S, Bronte V (Mar 2012) Coordinated regulation of myeloid cells by tumours. *Nat Rev Immunol* 12(4):253–268.
18. Szomolay B, Eubank TD, Roberts RD, Marsh CB, Friedman A (June 2012) Modeling the inhibition of breast cancer growth by gm-csf. *J Theor Biol* 303:141–151.
19. Chanmee T, Ontong P, Konno K, Itano N (Augest 2014) Tumor-associated macrophages as major players in the tumor microenvironment. *Cancers* 6(3):1670–1690.
20. Shu S, Polyak K (Jan 6, 2017) Bet bromodomain proteins as cancer therapeutic targets. *Cold Spring Harb Symp Quant Biol* pii: 030908:doi: 10.1101/sqb.2016.81.030908.
21. da Motta LL, et al. (Jan 2017) The bet inhibitor jq1 selectively impairs tumour response to hypoxia and downregulates ca9 and angiogenesis in triple negative breast cancer. *Oncogene* 36(1):122–132.
22. Markowitz J, Wesolowski R, Papenfuss T, Brooks TR, Carson WE (July 2013) Myeloid-derived suppressor cells in breast cancer. *Breast Cancer Res Treat* 140(1):13–21.
23. Mautea RL, et al. (Nov 2015) Engineering high-affinity pd-1 variants for optimized immunotherapy and immuno-pet imaging. *Proc Natl Acad Sci USA* 112(47):E6506–14.
24. Cheng X, et al. (Apr 2013) Structure and interactions of the human programmed cell death 1 receptor. *J Biol Chem* 288(17):11771–11785.
25. Hao W, Friedman A (Apr 2016) Serum upar as biomarker in breast cancer recurrence: A mathematical model. *PLoS ONE* 11(4):e0153508.
26. Young ME (1980) Estimation of diffusion coefficients of proteins. *Biotechnology and Bioengineering* XXII:947–955.
27. Shui YB, et al. (2003) Vascular endothelial growth factor expression and signaling in the lens. *Invest Ophthalmol Vis Sci* 44(9):3911–3919.
28. Liao KL, Bai XF, Friedman A (2014) Mathematical modeling of interleukin-27 induction of anti-tumor t cells response. *PLoS ONE* 9(3):e91844.
29. PhosphoSitePlus/ (2003) Il2 (human), http://www.phosphosite.org/proteinaction?id=14691&showallsites=true.
30. Hamza T, Barnett JB, Li B (Feb 2010) Interleukin 12 a key immunoregulatory cytokine in infection applications. *Int J Mol Sci* 11(3):789–806.
31. Poniatowski LA, Wojdasiewicz P, Gasik R, Szukiewicz D (2015) Transforming growth factor beta family: Insight into the role of growth factors in regulation of fracture healing biology and potential clinical applications. *Mediators of Inflammation* 2015(Article ID 137823):1–17.
32. PhosphoSitePlus/ (2003) Il10(human), http://www.phosphosite.org/proteinaction.action?id=2473887.
33. PhosphoSitePlus/ (2003) Tnf-a (human), http://www.phosphosite.org/proteinaction?id=8542247&showallsites=true.
34. PhosphoSitePlus/ (2003) M-csf (human), http://www.phosphosite.org/proteinaction?id=15907&showallsites=true.
35. PhosphoSitePlus/ (2003) Ccl2 (human), http://www.phosphosite.org/proteinaction?id=14083910&showallsites=true.
36. Longoria TC, Tewari KS (Oct 2016) Evaluation of the pharmacokinetics and metabolism of pembrolizumab in the treatment of melanoma. *Expert Opin Drug Metab Toxicol* 12(10):1247–1253.
37. Abcam/ (1998) (+)-jq1 (ab141498), http://www.abcam.com/-jq1-ab141498.html.
38. Steptoe RJ, Patel RK, Subbotin VM, Thomson AW (2000) Comparative analysis of dendritic cell density and total number in commonly transplanted organs: morphometric estimation in normal mice. *Transpl Immunol* 8(1):49–56.
39. Bergstresser PR, Fletcher CR, Streilein JW (1980) Surface densities of langerhans cells in relation to rodent epidermal sites with special immunologic properties. *J Invest Dermatol* 74(2):77–88.
40. Romani N, Clausen BE, Stoitzner P (March 2010) Langerhans cells and more: langerin-expressing dendritic cell subsets in the skin. *Immunol Rev* 234(1):120–141.
41. Dumortier H, et al. (2005) Antigen presentation by an immature myeloid dendritic cell line does not cause ctl deletion in vivo, but generates cd8+ central memory-like t cells that can be rescued for full effector function. *J Immunol* 175(2):855–863.
42. Ataera H, Hyde E, Price KM, Stoitzner P, Ronchese F (March 2011) Murine melanoma-infiltrating dendritic cells are defective in antigen presenting function regardless of the presence of cd4cd25 regulatory t cells. *PLoS One* 6(3):e17515.
43. Hao W, Friedman A (2017) The role of exosomes in pancreatic cancer microenvironment. *Bull Math Biol* https://doi.org/10.1007/s11538-017-0254-9.
44. Hussein MR (Jun 2006) Tumour-associated macrophages and melanoma tumourigenesis: integrating the complexity. *Int J Exp Pathol* 87(3):163–176.
45. Hao W, Rovin BH, , Friedman A (September 2014) Mathematical model of renal interstitial fibrosis. *Proc Natl Acad Sci U S A* 111(39):14193–14198.
46. Chen D, et al. (Oct 2014) Involvement of tumor macrophage hifs in chemotherapy effectiveness: mathematical modeling of oxygen, ph, and glutathione. *PLoS ONE* 9(10):e107511.
47. Chun Y, et al. (2008) Elevated interleukin-12 is a plasma marker of poor prognosis in stage iii melanoma patients. *American Assosiation for Cancer Research* AACR Meeting 2008(Abstract 5568).
48. Bankhead C (2008) Aacr: Il-12 level may predict melanoma prognosis. *Medpage Today* p. http://www.medpagetoday.com/meetingcoverage/aacr/9177.
49. Kaminska B, Wesolowska A, Danilkiewicz M (2005) Tgf beta signalling and its role in tumour pathogenesis. *Acta Biochim Pol* 52(2):329–337.
50. Kyrtsonis MC, et al. (1998) Serum transforming growth factor-beta 1 is related to the degree of immunoparesis in patients with multiple myeloma. *Med Oncol* 15(2):124–128.
51. Mueller C, et al. (2009) The pros and cons of immunomodulatory il-10 gene therapy with recombinant aav in a cftr-/–dependent allergy mouse model. *Gene Therapy* 16:172–183.
52. Nemunaitis J, Fong T, Shabe P, Martineau D, Ando D (2001) Comparison of serum interleukin-10 (il-10) levels between normal volunteers and patients with advanced melanoma. *Cancer Invest* 19(3):239–247.
53. Itakura E, et al. (June 2011) Il-10 expression by primary tumor cells correlates with melanoma progression from radial to vertical growth phase and development of metastatic competence. *Mod Pathol* 24(6):801–809.
54. Oliver JC, et al. (1993) Cytokine kinetics in an in vitro whole blood model following an endotoxin challenge. *Lymphokine Cytokine Res* 12(2):115–120.
55. Lo WC, Arsenescu V, Arsenescu RI, , Friedman A (November 2016) Inflammatory bowel disease: How effective is tnf-alpha suppression? *PLoS One* 11(11):e0165782.
56. Siewe N, Yakubu AA, Satoskar AR, Friedman A (Jan 2017) Granuloma formation in leishmaniasis: A mathematical model. *J Theor Biol* 412:48–60.
57. Hao W, Schlesinger LS, Friedman A (March 17, 2016) Modeling granulomas in response to infection in the lung. *PLoS ONE* 11(3):e0148738.
58. Agata Y, et al. (1996) Expression of the pd-1 antigen on the surface of stimulated mouse t and b lymphocytes. *Int Immunol* 8(5):765–772.
59. Cheng X, et al. (2017) Human pd-l1/b7-h1/cd274 protein. *Sino Biological Inc, http://www.sinobiological.com/PD-L1-B7-H1-CD274-Protein-g-533.html.*
60. Linsley PS, et al. (1992) Coexpression and functional cooperation of ctla-4 and cd28 on activated t lymphocytes. *J Exp Med* 176(6):1595–1604.
61. Lai X, Friedman A (July 2017) Combination therapy of cancer with braf inhibitor and immune checkpoint inhibitor: A mathematical model. *BMC Syst Biol.* 11(1):70.
62. Fellner C (2012) Ipilimumab (yervoy) prolongs survival in advanced melanoma. *P T.* 37(9):503–511.
63. Trabucco SE, et al. (Jan 2015) Inhibition of bromodomain proteins for the treatment of human diffuse large b-cell lymphoma. *Clin Cancer Res* 21(1):113–122.
64. Moyer MW (Nov 2011) First drugs found to inhibit elusive cancer target. *Nat Med* 17(11):1325.
65. Marino S, Hogue I, Ray C, Kirschner D (2008) A methodology for performing global uncertainty and sensitivity analysis in systems biology. *J Theor Biol* 254(1):178–196.
66. Shi L, Chen S, Yang L, Li Y (Sep 2013) The role of pd-1 and pd-l1 in t-cell immune suppression in patients with hematological malignancies. *J Hematol Oncol* 6(74):doi: 10.1186/1756–8722–6–74.
67. Muppidi MR, George S (2015) Immune checkpoint inhibitors in renal cell carcinoma. *Journal of Targeted Therapies in Cancer 2015* 4:47–52.
68. Cooper ZA, et al. (July 2014) Response to braf inhibition in melanoma is enhanced when combined with immune checkpoint blockade. *Cancer Immunol Res* 2(7):643–654.
69. Hogg SJ, et al. (Feb 2017) Bet-bromodomain inhibitors engage the host immune system and regulate expression of the immune checkpoint ligand pd-l1. *Cell Rep* 18(9):2162–2174.
70. Munn DH, Mellor AL (March 2016) Ido in the tumor microenvironment: Inflammation, counter-regulation, and tolerance. *Trends in Immunology* 37(3):193–207.
71. Francisco LM, Sage PT, , Sharpe AH (2010) The pd-1 pathway in tolerance and autoimmunity. *Immunol Rev* 236:219–242.
72. Zhu H, et al. (September 2017) Bet bromodomain inhibition promotes anti-tumor immunity by suppressing pd-l1 expression. *Cell Rep* 16(11):2829–2873.
73. Lowther DE, et al. (Apr 2016) Pd-1 marks dysfunctional regulatory t cells in malignant gliomas. *JCI Insight* 1(5):e85935.
74. Buttea MJ, Pena-Cruzc V, Kima MJ, Freemanc GJ, Sharpe AH (Aug 2008) Interaction of human pd-l1 and b7-1. *Mol Immunol* 45(13):3567–3572.
75. Brahmer JR, et al. (Jun 2012) Safety and activity of anti-pd-l1 antibody in patients with advanced cancer. *N Engl J Med* 366(26):2455–2465.
76. Mertz JA, et al. (2011) Targeting myc dependence in cancer by inhibiting bet bromodomains. *Proc Natl Acas Sci U S* 108(40):16669–16674.
77. Bian B, et al. (Apr 2017) Gene expression profiling of patient-derived pancreatic cancer xenografts predicts sensitivity to the bet bromodomain inhibitor jq1: implications for individu-

Table S1. List of variables (in units of g/cm^3).

Notation	Description	Notation	Description
D	density of DCs	T_α	TNF-α concentration
T_1	density of activated CD4^+ T cells	N	NO concentration
T_8	density of activated CD8^+ T cells	W	Oxygen density
T_r	density of activated Treg cells	G	VEGF concentration
M_1	density of M1	M_C	M-CSF concentration
M_2	density of M2	M_P	MCP-1 concentration
E	density of Endothelial cells	P	PD-1 concentration
C	density of cancer cells	L	PD-L1 concentration
I_{12}	IL-12 concentration	Q	PD-1-PD-L1 concentration
I_2	IL-2 concentration	A	anti-PD-L1 concentration
T_β	TGF-β concentration	B	BET inhibitor concentration
I_{10}	IL-10 concentration		

alized medicine efforts. *EMBO Mol Med* 9(4):482–497.

78. D'Acunto B (2004) *Computational Methods for PDE in mechanics*, Series on Advances in Mathematics for Applied Sciences-Vol.67. (Word Scientific, Singapore).
79. Kim Y, Lawler S, Nowicki MO, Chiocca EA, Friedman A (Oct 2009) A mathematical model for pattern formation of glioma cells outside the tumor spheroid core. *J Theor Biol* 260(3):359–371.
80. Kim Y, Wallace J, Li F, Ostrowski M, Friedman A (Sep 2010) Transformed epithelial cells and fibroblasts/myofibroblasts interaction in breast tumor: a mathematical model and experiments. *J Theor Biol* 61(3):401–421.
81. Hao W, Friedman A (Nov 18, 2016) Mathematical model on alzheimer's disease. *BMC Syst Biol* 10(108):1–18.
82. Hao W, et al. (2017) A mathematical model of chronic pancreatitis. *Proc Natl Acas Sci U S* 114(19):5011–5016.

Table S2. Summary of parameter values

Notation	Description	Value used	References
δ_D	diffusion coefficient of DCs	8.64×10^{-7} cm^2 day^{-1}	(43)
δ_T	diffusion coefficient of T cells	8.64×10^{-7} cm^2 day^{-1}	(43)
δ_M	diffusion coefficient of macrophages	8.64×10^{-7} cm^2 day^{-1}	(43)
δ_E	diffusion coefficient of endothelial cells	8.64×10^{-7} cm^2 day^{-1}	(43)
δ_C	diffusion coefficient of tumor cells	8.64×10^{-7} cm^2 day^{-1}	(43)
$\delta_{I_{12}}$	diffusion coefficient of IL-12	6.05×10^{-2} cm^2 day^{-1}	estimated
δ_{I_2}	diffusion coefficient of IL-2	9.58×10^{-2} cm^2 day^{-1}	estimated
δ_{T_β}	diffusion coefficient of TGF-β	8.52×10^{-2} cm^2 day^{-1}	estimated
$\delta_{I_{10}}$	diffusion coefficient of IL-10	9.11×10^{-2} cm^2 day^{-1}	estimated
δ_{T_α}	diffusion coefficient of TNF-α	8.46×10^{-2} cm^2 day^{-1}	estimated
δ_W	diffusion coefficient of oxygen	1.728 cm^2 day^{-1}	(46)
δ_N	diffusion coefficient of NO	1.728 cm^2 day^{-1}	(46)
δ_G	diffusion coefficient of VEGF	8.64×10^{-2} cm^2 day^{-1}	(28)
δ_{M_C}	diffusion coefficient of M-CSF	6.36×10^{-2} cm^2 day^{-1}	estimated
δ_{M_P}	diffusion coefficient of MCP-1	1.12×10^{-1} cm^2 day^{-1}	estimated
δ_A	diffusion coefficient of anti-PD-L1	4.73×10^{-2} cm^2 day^{-1}	estimated
δ_B	diffusion coefficient of BETi	3.24×10^{-1} cm^2 day^{-1}	estimated
σ_0	flux rate of T_1 and T_8 cells at the boundary	1 cm^{-1}	(43)
χ_M	chemoattraction coefficient of MCP-1	10 cm^5/g $\cdot$ day	(79, 80)
χ_G	chemoattraction coefficient of VEGF	10 cm^5/g $\cdot$ day	(79, 80)
λ_{DC}	activation rate of DCs by tumor cells	7.4 g/cm^3 $\cdot$ day	estimated
$\lambda_{T_1 I_{12}}$	activation rate of CD4$^+$ T cells by IL-12	27.96 day^{-1}	estimated
$\lambda_{T_1 I_2}$	activation rate of CD4$^+$ T cells by IL-2	0.25 day^{-1}	(43)
$\lambda_{T_8 I_{12}}$	activation rate of CD8$^+$ T cells by IL-12	24.90 day^{-1}	estimated
$\lambda_{T_8 I_2}$	activation rate of CD8$^+$ T cells by IL-2	0.25 day^{-1}	(43)
$\lambda_{T_r T_\beta}$	activation rate of Tregs by TGF-β	1.5day^{-1}	estimated
λ_{M_1}	activation rate of M1 macrophages	1.35 day^{-1}	estimated
λ_{M_2}	activation rate of M2 macrophages	1.01 day^{-1}	estimated
β_{M_1}	phenotype change rate of M1 to M2 macrophages	0.15 day^{-1}	estimated
β_{M_2}	phenotype change rate of M2 to M1 macrophages	2.34×10^{-3} day^{-1}	estimated
λ_E	activation rate of endothelial cells	2.38×10^{7} day^{-1}	estimated
λ_C	growth rate of cancer cells	1.92 day^{-1}	estimated
$\lambda_{I_{12}D}$	production rate of IL-12 by DCs	1.38×10^{-6} day^{-1}	estimated
$\lambda_{I_{12}M_1}$	production rate of IL-12 by M1 macrophages	5.52×10^{-6} day^{-1}	estimated
$\lambda_{I_2 T_1}$	production rate of IL-2 by CD4$^+$ T cells	2.82×10^{-8} day^{-1}	(43)
$\lambda_{T_\beta C}$	production rate of TGF-β by cancer cells	5.39×10^{-11} day^{-1}	estimated
$\lambda_{T_\beta T_r}$	production rate of TGF-β by Tregs	2.16×10^{-7} day^{-1}	(55)
$\lambda_{T_\beta M_2}$	production rate of TGF-β by M2 macrophages	1.35×10^{-9} day^{-1}	estimated
$\lambda_{I_{10}C}$	production rate of IL-10 by cancer cells	2.07×10^{-8} day^{-1}	estimated
$\lambda_{I_{10}M_2}$	production rate of IL-10 by M2 macrophages	1.65×10^{-9} day^{-1}	estimated
$\lambda_{T_\alpha M_1}$	production rate of TNF-α by M1 macrophages	1.36×10^{-5} day^{-1}	estimated
$\lambda_{T_\alpha T_1}$	production rate of TNF-α by Th1 cells	1.36×10^{-7} day^{-1}	estimated
$\lambda_{N M_2}$	production rate of NO by M2 macrophages	0.12/day	estimated
$\lambda_{W E}$	production rate of oxygen by endothelial cells	7×10^{-2}/day	(25)
λ_{GC}	production rate of VEGF by cancer cells	2×10^{-6} day^{-1}	(25)
$\lambda_{G M_2}$	production rate of VEGF by M2 macrophages	2.5×10^{-5} day^{-1}	estimated
$\lambda_{M_C C}$	production rate of M-CSF by cancer cells	1.2×10^{-8} day^{-1}	estimated
$\lambda_{M_P M_2}$	production rate of MCP-1 by M2 macrophages	1.2×10^{-8} day^{-1}	estimated
$\lambda_{M_P C}$	production rate of MCP-1 by cancer cells	8.24×10^{-7} day^{-1}	estimated

Table S3. Summary of parameter values

Notation	Description	Value used	References
d_D	death rate of DCs	0.1 day^{-1}	(43)
d_{T_1}	death rate of CD4$^+$ T cells	0.197 day^{-1}	(43)
d_{T_8}	death rate of CD8$^+$ T cells	0.18 day^{-1}	(43)
d_{T_r}	death rate of Tregs	0.2 day^{-1}	(55)
d_{M_1}	death rate of M1 macrophage	0.015 day^{-1}	(81)
d_{M_2}	death rate of M2 macrophage	0.015 day^{-1}	(81)
d_E	death rate of endothelial cells	0.69 day^{-1}	(43)
d_C	death rate of tumor cells	0.17 day^{-1}	(43)
$d_{I_{12}}$	degradation rate of IL-12	1.38 day^{-1}	(43)
d_{I_2}	degradation rate of IL-2	2.376 day^{-1}	(43)
d_{T_β}	degradation rate of TGF-β	499.066 day^{-1}	estimated
$d_{I_{10}}$	degradation rate of IL-10	8.3178 day^{-1}	estimated
d_{T_α}	degradation rate of TGF-α	55.01 day^{-1}	estimated
d_N	degradation rate of NO	198 day^{-1}	(56)
d_W	take-up rate of oxygen by cells	3.76×10^{-1} day^{-1}	(25)
d_G	degradation rate of VEGF	12.6 day^{-1}	(25)
d_{M_C}	degradation rate of M-CSF	4.8/day	(25)
d_{M_P}	degradation rate of MCP-1	55.01 day^{-1}	(25)
d_A	degradation rate of anti-PD-L1	0.047 day^{-1}	estimated
d_B	degradation rate of BETi	13.86 day^{-1}	estimated
K_D	half-saturation of CD4$^+$ T cells	4×10^{-4} $\mathrm{g/cm}^3$	estimated
K_{T_1}	half-saturation of CD4$^+$ T cells	2×10^{-3} $\mathrm{g/cm}^3$	estimated
K_{T_8}	half-saturation of CD8$^+$ T cells	1×10^{-3} $\mathrm{g/cm}^3$	estimated
K_{T_r}	half-saturation of Tregs	5×10^{-4} $\mathrm{g/cm}^3$	(43)
K_{M_1}	half-saturation of M1 macrophages	10^{-4} $\mathrm{g/cm}^3$	estimated
K_{M_2}	half-saturation of M2 macrophages	3.2×10^{-3} $\mathrm{g/cm}^3$	estimated
K_E	half-saturation of endothelial cells	2.5×10^{-3} $\mathrm{g/cm}^3$	(25)
K_C	half-saturation of tumor cells	0.4 $\mathrm{g/cm}^3$	(43)
$K_{I_{12}}$	half-saturation of IL-12	8×10^{-10} $\mathrm{g/cm}^3$	estimated
K_{I_2}	half-saturation of IL-2	2.37×10^{-11} $\mathrm{g/cm}^3$	(43)
K_{T_β}	half-saturation of TGF-β	2.68×10^{-13} $\mathrm{g/cm}^3$	estimated
$K_{I_{10}}$	half-saturation of IL-10	8.75×10^{-11} $\mathrm{g/cm}^3$	estimated
K_{T_α}	half-saturation of α	3×10^{-11} $\mathrm{g/cm}^3$	(82)
K_N	half-saturation of NO	2×10^{-6} $\mathrm{g/cm}^3$	(56)
K_W	half-saturation of oxygen	4.65×10^{-4} $\mathrm{g/cm}^3$	(25)
K_G	half-saturation of VGEF	7×10^{-8} $\mathrm{g/cm}^3$	(25)
K_{M_C}	half-saturation of M-CSF	10^{-9} $\mathrm{g/cm}^3$	(25)
K_{M_P}	half-saturation of MCP-1	2×10^{-7} $\mathrm{g/cm}^3$	(25)
K_B	half-saturation of BETi	8.02×10^{-11} $\mathrm{g/cm}^3$	estimated
$K_{TI_{10}}$	inhibition of function of T cells by IL-10	4.375×10^{-11} $\mathrm{g/cm}^3$	estimated
K_{TT_r}	inhibition of function of T cells by Tregs	$2,5 \times 10^{-4}$ $\mathrm{g/cm}^3$	estimated
K_{TN}	inhibition of function of T cells by NO	2×10^{-6} $\mathrm{g/cm}^3$	estimated
K'_{TQ}	inhibition of function of T cells by PD-1-PD-L1	4.86×10^{-20} $\mathrm{g}^2/\mathrm{cm}^6$	estimated
K_{CB}	inhibition of proliferation of cancer cells by BETi	8.02×10^{-10} $\mathrm{g/cm}^3$	estimated
$K_{T_\alpha B}$	inhibition of production of TNF-α by BETi	8.02×10^{-10} $\mathrm{g/cm}^3$	estimated
K_{GB}	inhibition of production of VEGF by BETi	8.02×10^{-10} $\mathrm{g/cm}^3$	estimated
$K_{T_r B}$	inhibition of Tregs by BETi	8.02×10^{-10} $\mathrm{g/cm}^3$	estimated

Table S4. Summary of parameter values

Notation	Description	Value used	References
D_0	density of inactive DCs	2×10^{-5} g/cm^3	(43)
T_{10}	density of naive CD4$^+$ T cells in tumor	4×10^{-4} g/cm^3	estimated
T_{80}	density of naive CD8$^+$ T cells in tumor	2×10^{-4} g/cm^3	estimated
M_{10}	density of monocytes	1.2×10^{-4} g/cm^3	estimated
M_{20}	density of monocytes	3.84×10^{-3} g/cm^3	estimated
C_M	carrying capacity of cancer cells	0.8 g/cm^3	(43)
$\hat{T}_1$	density of CD4$^+$ T cells from lymph node	4×10^{-3} g/cm^3	estimated
$\hat{T}_8$	density of CD8$^+$ T cells from lymph node	2×10^{-3} g/cm^3	estimated
$\hat{T}_r$	density of CD8$^+$ T cells from lymph node	1×10^{-3} g/cm^3	estimated
E_M	carrying capacity of endothelial cells	5×10^{-3} g/cm^3	(25)
G_0	threshold of VEGF concentration	3.65×10^{-10} g/cm^3	(25)
W_G	threshold of oxygen density	10^{-4} g/cm^3	(25)
η_1	killing rate of tumor cells by CD4$^+$ T cells	65.71 cm^3/g $\cdot$ day	estimated
η_8	killing rate of tumor cells by CD8$^+$ T cells	328.55 cm^3/g $\cdot$ day	estimated
μ_{LA}	blocking rate of PD-L1 by anti-PD-1	1.09×10^6 cm^3/g $\cdot$ day	estimated
μ_{BC}	absorbtion rate of BETi by cancer cells	6.17×10^{-9} day^{-1}	estimated
μ_{BM_1}	absorbtion rate of BETi by M1 macrophages	6.17×10^{-9} day^{-1}	estimated
ρ_P	expression of PD-1 in T cells	2.49×10^{-7}	estimated
ρ_L	expression of PD-L1 in T cells	3.25×10^{-7}	estimated
ε_B	Promotion of effector T cells by BETi	2×10^{10} cm^3/g	estimated